

Coding of Nonlinear States for NLS-Type Equations with Periodic Potential

G.L. Alfimov and A.I. Avramenko

Abstract The problem of complete description of nonlinear states for NLS-type equations with periodic potential is considered. We show that in some cases all nonlinear states for equations of such kind can be coded by bi-infinite sequences of symbols of N -symbol alphabet (*words*). Sufficient conditions for one-to-one correspondence between the set of nonlinear states and the set of these bi-infinite words are given in the form convenient for numerical verification (Hypotheses 1–3). We report on numerical check of these hypotheses for the case of Gross-Pitaevskii equation with cosine potential and indicate regions in the space of governing parameters where this coding is possible.

1 Introduction

The model equation

$$u_{xx} + (\mu - V(x))u - F(u) = 0, \quad \mu \in \mathbb{R}, \quad V(x), u(x) \in \mathbb{R} \quad (1)$$

where $V(x)$ is a periodic function, has been widely used to study steady states in nonlinear periodic media. In particular, Eq. (1) describes nonlinear modes

$$\psi(x, t) = \exp(-i\mu t)u(x) \quad (2)$$

for NLS-type equation

$$i\psi_t = -\psi_{xx} + f(|\psi|^2)\psi + V(x)\psi. \quad (3)$$

G.L. Alfimov (✉) · A.I. Avramenko

National Research University of Electronic Technology, Zelenograd, Moscow, 124498, Russia
e-mail: galfimov@yahoo.com; avramenkoaleksey@gmail.com

Equation (3) arises in various physical applications such as optics, plasma physics and theory of Bose-Einstein condensation (BEC). In BEC context μ has the sense of chemical potential and $\psi(x, t)$ describes the macroscopic wave function. The periodic potential $V(x)$ corresponds to an optical trap to confine the condensate, see the surveys [1–3]. Let us give some examples.

- (i) The classical version of Eq. (3) corresponds to the case $f(\xi) = g\xi$ where $g = \pm 1$ (both the signs “+” and “−” are admissible from physical viewpoint). In this case Eq. (3) becomes the Gross-Pitaevskii equation [4]

$$i\psi_t = -\psi_{xx} + g|\psi|^2\psi + V(x)\psi. \quad (4)$$

The case $g = 1$ corresponds to repulsive interparticle interactions, $g = -1$ – to attractive interactions. Using ansatz (2) and assuming that $u(x)$ is real we arrive at the following version of Eq. (1)

$$u_{xx} + (\mu - V(x))u - gu^3 = 0. \quad (5)$$

- (ii) In order to describe complex nonlinear modes for Eq. (4) one can separate amplitude and phase of the solution and use the substitution

$$\psi(x, t) = u(x) \exp\{-i(\mu t + \phi(x))\}$$

instead of (2). Then one arrives at the equation for the amplitude $u(x)$

$$u_{xx} + (\mu - V(x))u - gu^3 - \frac{M^2}{u^3} = 0, \quad (6)$$

where M is an arbitrary real constant [5]. The phase $\phi(x)$ can be found from the relation $u^2\phi_x = M$. Equation (6) is a particular case of Eq. (1) with $F(u) = gu^3 + M^2/u^3$.

- (iii) In some situations the cubic nonlinearity in (4) must be replaced by a nonlinearity of more general type, for instance, quintic or cubic-quintic one [6, 7]. Taking $f(\xi) = g_1\xi + g_2\xi^2$ and assuming that $u(x)$ is real one arrives at the equation

$$u_{xx} + (\mu - V(x))u - g_1u^3 - g_2u^5 = 0. \quad (7)$$

It is known that even in the simplest case of cubic nonlinearity and model cosine potential

$$V(x) = A \cos 2x \quad (8)$$

Eq. (1) describes a great variety of nonlinear states. Among them are: bright and dark gap solitons [5, 8–10], nonlinear periodic structures (nonlinear Bloch waves) [8, 11],

domain walls [12], gap waves [13] and so on. However, to best of our knowledge, up to the moment a classification of all the possible types of nonlinear modes for Eq. (1) has not been constructed.

In the present contribution we address the problem of *complete description of nonlinear states* covered by Eq. (1). Our approach is based on the following observation: for some class of nonlinearities the “most part” of the solutions for Eq. (1) are *singular* i.e. they collapse (tend to infinity) at some finite point of real axis. In particular, such a situation takes place in the case of GPE with repulsive nonlinearity, $g = 1$, Eqs. (5), (6), and for cubic-quintic generalization of GPE if $g_2 > 0$, Eq. (7). In these cases the set of bounded in \mathbb{R} solutions for Eq. (1) is quite scanty, it can be found numerically by properly organized scanning of initial data plane for the Cauchy problem. Then the transformations of this initial data under the action of Poincaré map T can be interpreted in terms of symbolic dynamics.

This contribution is aimed to present a *general scheme* of the coding technique. The proofs of theorems are omitted (see the paper [14] for details). The main results are presented for Eq. (5) with $g = 1$, i.e.

$$u_{xx} + (\mu - V(x))u - u^3 = 0, \quad (9)$$

where $\mu, V(x), u(x) \in \mathbb{R}$ and the potential $V(x)$ is π -periodic. In Sect. 2 we introduce some notations and definitions which will be used throughout the rest of the text and formulate some statements about them. In Sect. 3 we formulate some statements from symbolic dynamics theory and apply them to describe the dynamics of iterated Poincaré map. The main outcome of Sect. 3 is formulated in a form of three Hypotheses. These Hypotheses give sufficient conditions for one-to-one correspondence between the bounded solutions of Eq. (9) and coding sequences. These conditions should be verified numerically. Section 4 contains application of this approach to the case of the cosine potential (8). Section 5 includes short summary and discussion.

2 Bounded and Singular Solutions of Stationary States

2.1 Some Definitions

In what follows we refer to a solution $u(x)$ of Eq. (9) as a *singular solution* if for some $x = x_0$

$$\lim_{x \rightarrow x_0} u(x) = +\infty \quad \text{or} \quad \lim_{x \rightarrow x_0} u(x) = -\infty.$$

In this case we say that the solution $u(x)$ *collapses* at x_0 . Also let us introduce the following definitions:

Collapsing and non-collapsing points: A point (u_0, u'_0) of the plane $\mathbb{R}^2 = (u, u')$ is

- *L-collapsing forward point*, $L > 0$, if the solution of Cauchy problem for Eq. (9) with initial data $u(0) = u_0$, $u_x(0) = u'_0$ collapses at value $x = x_0$ and $0 < x_0 < L$;
- *L-non-collapsing forward point*, $L > 0$, if the solution of Cauchy problem for Eq. (9) with initial data $u(0) = u_0$, $u_x(0) = u'_0$ does not collapse at any value $x = x_0$, $0 < x_0 \leq L$.
- *L-collapsing backward point* if the corresponding solution of Cauchy problem for Eq. (9) collapses at some value $x = -x_0$ and $0 < x_0 < L$;
- *L-non-collapsing backward point* if the corresponding solution of Cauchy problem for Eq. (9) does not collapse at any value $x = -x_0$, $0 < x_0 \leq L$;
- *A collapsing point* if it is either *L-collapsing forward point* or *L-collapsing backward point* for some L .

Functions $h^\pm(\tilde{u}, \tilde{u}')$. The functions $h^+(\tilde{u}, \tilde{u}')$ and $h^-(\tilde{u}, \tilde{u}')$ are defined in \mathbb{R}^2 as follows: $h^+(\tilde{u}, \tilde{u}') = x_0$ if the solution of Cauchy problem for Eq. (9) with initial data $u(0) = \tilde{u}$, $u_x(0) = \tilde{u}'$ collapses at value $x = x_0$, $x_0 > 0$. Similarly, $h^-(\tilde{u}, \tilde{u}') = -x_0$ if the solution of Cauchy problem for Eq. (9) with initial data $u(0) = \tilde{u}$, $u_x(0) = \tilde{u}'$ collapses at value $x = x_0$, $x_0 < 0$.

The sets \mathcal{U}_L^\pm and \mathcal{U}_L . We denote the set of all *L-non-collapsing forward points* by \mathcal{U}_L^+ and the set of all *L-non-collapsing backward points* by \mathcal{U}_L^- . In terms of the functions $h^\pm(u, u')$ these sets are

$$\mathcal{U}_L^+ = \{(u, u') \in \mathbb{R}^2 \mid h^+(u, u') > L\}, \quad \mathcal{U}_L^- = \{(u, u') \in \mathbb{R}^2 \mid h^-(u, u') > L\}.$$

The intersection of \mathcal{U}_L^+ and \mathcal{U}_L^- will be denoted by \mathcal{U}_L . Evidently, if $L_1 < L_2$ then $\mathcal{U}_{L_2}^+ \subset \mathcal{U}_{L_1}^+$, $\mathcal{U}_{L_2}^- \subset \mathcal{U}_{L_1}^-$ and $\mathcal{U}_{L_2} \subset \mathcal{U}_{L_1}$.

2.2 Some Statements About Collapsing Points

It turns out that the “most part” of the plane (u, u') of initial data are either *L-collapsing forward points* or *L-collapsing backward points* for some L . This follows from Theorem 1 below:

Theorem 1. *Let the potential $V(x)$ be continuous and bounded on \mathbb{R} . Then for each L there exist \tilde{u}_L and \tilde{u}'_L such that the set \mathcal{U}_L is situated in the rectangle $-\tilde{u}_L < u < \tilde{u}_L$, $-\tilde{u}'_L < u' < \tilde{u}'_L$.*

The proof of Theorem 1 is rather technical and can be found in [14]. Another important statement is as follows:

Theorem 2. *Let the potential $V(x)$ be continuous and bounded on \mathbb{R} and $h^+(u_0, u'_0) = L < \infty$. Then $h^+(u, u')$ is a continuous function in some vicinity of the point (u_0, u'_0) .*

The proof of Theorem 2 also is presented in [14]. It worth commenting Theorem 2 as follows:

- (i) Analogous statement is valid for the function $h^-(u, u')$;
- (ii) It follows from Theorem 2 that the boundary of the set \mathcal{U}_L^+ is continuous and corresponds to the level line $h^+(u, u') = L$ of the function $h^+(u, u')$. This boundary consists of the points (\tilde{u}, \tilde{u}') such that the solution of Eq. (9) with initial data $u(0) = \tilde{u}$, $u_x(0) = \tilde{u}'$ satisfies one of the conditions

$$\lim_{x \rightarrow L} u(x) = +\infty \quad \text{or} \quad \lim_{x \rightarrow L} u(x) = -\infty$$

Correspondingly, the boundary of the set \mathcal{U}_L^- is also continuous and consists of the points (\tilde{u}, \tilde{u}') such that the solution of Eq. (9) with initial data $u(0) = \tilde{u}$, $u_x(0) = \tilde{u}'$ satisfy one of the conditions

$$\lim_{x \rightarrow -L} u(x) = +\infty \quad \text{or} \quad \lim_{x \rightarrow -L} u(x) = -\infty$$

The set of solutions for Eq. (9) that collapse at given point $x = x_0$ can be described more precisely in terms of asymptotic expansions.

Theorem 3. *Let $x = x_0$ be an arbitrary fixed real. Assume that $U(x) = \omega - V(x)$ in a vicinity of $x = x_0$ can be represented as follows*

$$U(x) = U_0 + U_1\delta + U_2\delta^2 + U_3\delta^3 + o(\delta^3)$$

where $\delta \equiv x - x_0$. Then the solutions of Eq. (9) which satisfy the condition

$$\lim_{x \rightarrow x_0} u(x) = +\infty \tag{10}$$

obey the asymptotic expansion

$$u(\delta) = \frac{\sqrt{2}}{\delta} + A_1\delta + A_2\delta^2 + A_3\delta^3 \ln|\delta| + \mathbf{C}\delta^3 + A_4\delta^4 + o(\delta^4) \tag{11}$$

Here $\mathbf{C} \in \mathbb{R}$ is a free parameter and

$$A_1 = \frac{\sqrt{2}U_0}{6}; \quad A_2 = \frac{\sqrt{2}U_1}{4}; \quad A_3 = -\frac{\sqrt{2}U_2}{5}, \quad A_4 = \frac{\sqrt{2}}{6} \left(\frac{U_0U_1}{12} - U_3 \right)$$

The statement above follows from straightforward substitution of series (11) into Eq. (9). Theorem 3 should be commented as follows:

- (i) The free parameter \mathbf{C} is “internal” parameter of *continuous one-parameter set* of solutions which tend to $+\infty$ at the point $x = x_0$. This agrees well with the fact that the “most part” of solutions Eq. (9) are singular.
- (ii) Since Eq. (9) is invariant with respect to the symmetry $u \rightarrow -u$, the solutions of Eq. (9) which satisfy the condition

$$\lim_{x \rightarrow x_0} u(x) = -\infty$$

obey the same, up to sign, asymptotic expansion (11).

3 Periodic Potential: Poincaré Map

3.1 Poincaré Map

Assume now that the potential $V(x)$ is *continuous* and π -*periodic*

$$V(x + \pi) = V(x).$$

The prototypical example is the cosine potential (8) which appears as a basic model in numerous studies. Define the *Poincaré map* $T : \mathbb{R}^2 \rightarrow \mathbb{R}^2$ associated with Eq. (9) as follows: if $p = (\tilde{u}, \tilde{u}') \in \mathbb{R}^2$ then $Tp = (u(\pi), u_x(\pi))$ where $u(x)$ is a solution of Eq. (9) with initial data $u(0) = \tilde{u}$, $u_x(0) = \tilde{u}'$. The map T is an *area-preserving diffeomorphism*. It is important that T is defined *not* in the whole \mathbb{R}^2 , but only on the set of π -non-collapsing forward points for Eq. (9), i.e. \mathcal{U}_π^+ . Inverse map T^{-1} is defined on the set \mathcal{U}_π^- . Evidently, $T\mathcal{U}_\pi^+ = \mathcal{U}_\pi^-$.

If, in addition, the potential $V(x)$ is *even*, $V(x) = V(-x)$, Eq. (9) is reversible. Denote I the reflection with respect to u axis in the plane (u, u') . Due to reversibility of Eq. (9), if $p \in \mathcal{U}_\pi^+$ then $Ip \in \mathcal{U}_\pi^-$ and

$$T^{-1}Ip = ITp. \quad (12)$$

In general, the sets \mathcal{U}_π^+ and \mathcal{U}_π^- are connected by the relations $I\mathcal{U}_\pi^+ = \mathcal{U}_\pi^-$, $I\mathcal{U}_\pi^- = \mathcal{U}_\pi^+$. The set $\mathcal{U}_\pi = \mathcal{U}_\pi^+ \cap \mathcal{U}_\pi^-$ consists of the points which has both T -image and T -pre-image. It follows from Sect. 2 that \mathcal{U}_π is bounded.

We call *an orbit* a sequence of points (finite, infinite or bi-infinite) $\{p_n\}$, such that $Tp_n = p_{n+1}$. The fixed points of T correspond to π -periodic solutions of Eq. (9). These solutions do exist for quite general periodic potential $V(x)$, see [15]. For a fixed point p let us denote DT_p the operator of linearization of T at p . Denote $\lambda_{1,2}$ the eigenvalues of DT_p . Since the map is area-preserving, $\lambda_1\lambda_2 = 1$. Depending on the behavior of T in a vicinity of a fixed point, it may be of elliptic or hyperbolic type [16]. In the case of hyperbolic fixed point both $\lambda_{1,2}$ are real and in the case of

the elliptic point they are complex conjugated, $|\lambda_{1,2}| = 1$. Also we call a k -cycle of T an orbit which consists of points $p_1, \dots, p_k \in \mathbb{R}^2$ such that

$$Tp_1 = p_2, \quad Tp_2 = p_3, \dots, \quad Tp_k = p_1.$$

Evidently p_1 is a fixed point for T^k . The k -cycles correspond to $k\pi$ -periodic solutions of Eq. (9). A k -cycle is elliptic if p_1 is an elliptic fixed point for T^k and it is hyperbolic if p_1 is a hyperbolic fixed point for T^k .

The orbits of interest for this study are those which are (i) bi-infinite and (ii) remain within the set \mathcal{U}_π for any $n \in \mathbb{Z}$.

3.2 Symbolic Dynamics: Theory

Let (u, u') be Cartesian coordinates in \mathbb{R}^2 and $\nu(S)$ be a measure of set S in \mathbb{R}^2 . Let us remind that the function $f(u)$ is γ -Lipschitz function on some interval $J \in \mathbb{R}$ if for any $u_1, u_2 \in J$ the relation holds

$$|f(u_2) - f(u_1)| \leq \gamma |u_2 - u_1|.$$

Introduce the following definitions.

Definition. We call an island a curvilinear quadrangle D formed by nonintersecting curve segments $\alpha^+, \beta^+, \alpha^-, \beta^-$ (α^+ and α^- are opposite sides of the quadrangle and have no common points as well as β^+ and β^-) such that

- The segments α^+ and α^- are graphs of monotone non-decreasing/non-increasing γ -Lipschitz functions $u' = v_\pm(u)$ for some γ ;
- The segments β^+ and β^- are graphs of monotone non-increasing/non-decreasing γ -Lipschitz functions $u = h_\pm(u')$ for the same γ ;
- If $v_\pm(u)$ are monotone non-decreasing functions then $h_\pm(u)$ are monotone non-increasing functions and vice versa.

Definition. Let γ be a fixed real and D be an island bounded by curve segments $\alpha^+, \beta^+, \alpha^-, \beta^-$. We call v -curve a curve segment β with endpoints on α^- and α^+ which is

- A graph of monotone non-decreasing γ -Lipschitz function $u' = v(u)$ if β^\pm are graphs of monotone non-decreasing functions;
- A graph of monotone non-increasing γ -Lipschitz function $u' = v(u)$ if β^\pm are graphs of monotone non-increasing functions.

Similarly, we call h -curve a curve segment α with endpoints on β^- and β^+ which

- Is a graph of monotone non-decreasing γ -Lipschitz function $u = h(u')$ if α^\pm are graphs of monotone non-decreasing functions;

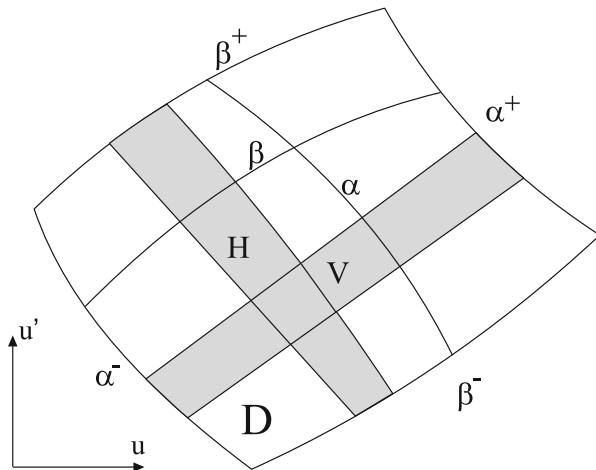


Fig. 1 An island D with v -curve β , v -strip V , h -curve α and h -strip H

- Is a graph of monotone non-increasing γ -Lipschitz function $u = h(u')$ if α^\pm are graphs of monotone non-increasing functions.

Definition. Let D be an island. We call v -strip an area concluded between two nonintersecting v -curves. Similarly, we call h -strip an area concluded between two nonintersecting h -curves.

Comment. According to the given definition of island any island is both h -strip and v -strip simultaneously.

Figure 1 illustrates schematically the definitions introduced above.

Let T be a diffeomorphism defined on a set $D = \bigcup_{i=1}^N D_i$ where each D_i , $i = 1, \dots, N$ is an island and all the islands are disjoint. Introduce the set \mathcal{P} of bi-infinite orbits $\{\dots, p_{-1}, p_0, p_1, \dots\}$, $Tp_i = p_{i+1}$, where all p_i , $i = 0, \pm 1, \pm 2, \dots$ belong to D . Let us denote Ω^N the set of bi-infinite sequences $\{\dots, i_{-1}, i_0, i_1, \dots\}$ where $i_k \in \{1, 2, \dots, N\}$. Define a map $\Sigma : \mathcal{P} \rightarrow \Omega^N$ as follows: i_k is the number i of the component D_i where the point p_k lies. Evidently, each orbit from \mathcal{P} defines uniquely a sequence from Ω^N . However, under some conditions each element from Ω^N also defines uniquely an orbit from \mathcal{P} , therefore Σ establishes one-to-one correspondence between \mathcal{P} and Ω^N . The following statement is valid:

Theorem 4. Assume that a diffeomorphism T is defined on a set of N disjoint islands D_i , $i = 1, \dots, N$, $D = \bigcup_{i=1}^N D_i$. Assume that:

- For any i , $i = 1, \dots, N$, and for each v -strip $V \in D_i$ the intersection $TV \cap D_j$, $j = 1, \dots, N$ is non-empty and is also a v -strip. Similarly, for any i , $i = 1, \dots, N$, and for each h -strip $H \in D_i$ the intersection $T^{-1}H \cap D_j$, $j = 1, \dots, N$ is non-empty and is also an h -strip.
- Denote

$$\begin{aligned}\Delta_0^+ &= D, & \Delta_n^+ &= T\Delta_{n-1}^+ \cap D, \\ \Delta_0^- &= D, & \Delta_n^- &= T^{-1}\Delta_{n-1}^- \cap D.\end{aligned}$$

Then

$$\lim_{n \rightarrow \infty} \nu(\Delta_n^+) = 0, \quad \lim_{n \rightarrow \infty} \nu(\Delta_n^-) = 0.$$

Then each element $\mathbf{s} \in \Omega^N$ defines uniquely an orbit $\mathbf{p} \in \mathcal{P}$ such that $\Sigma \mathbf{p} = \mathbf{s}$.

Theorems of such kind are well-known in dynamical system theory. The conditions (i)–(ii) can be viewed as some version of Conley-Moser conditions [16]. In particular, Theorem 4 allows to describe coding of orbits for Smale horseshoe [16] (in this case $N = 2$). The proof of Theorem 4 is presented in [14].

3.3 Symbolic Dynamics: Application

Basing on Theorem 4 a strategy for coding of bounded solutions for Eq. (9) would consist in verifying the following hypotheses.

Hypothesis 1. The set \mathcal{U}_π consists of N disjoint islands D_i , $i = 1, \dots, N$, i.e. of N curvilinear quadrangles bounded by curves which possess some monotonic properties (see Sect. 3.2).

Hypothesis 2. The Poincaré map T associated with Eq. (9) is such that

- (a) T maps v-strips of any D_i , $i = 1, \dots, N$, in such a way that for any v-strip V , $V \in D_i$, all the intersections $TV \cap D_j$, $j = 1, \dots, N$, are nonempty and are v-strips.
- (b) the inverse map T^{-1} maps h-strips of any D_i , $i = 1, \dots, N$, in such a way that for any h-strip H , $H \in D_i$, the intersections $T^{-1}H \cap D_j$, $j = 1, \dots, N$, are nonempty and are h-strips.

Comment. If the periodic potential $V(x)$ is *even* the point (b) of Hypothesis 2 follows from the point (a). In fact, if H is an h-strip then IH is a v-strip where I is a reflection with respect to ψ axis. Then the statement (b) follows from the relation (12).

Hypothesis 3. The sequences of sets Δ_n^\pm defined as follows

$$\begin{aligned}\Delta_0^+ &= \mathcal{U}_\pi, & \Delta_n^+ &= T\Delta_{n-1}^+ \cap \mathcal{U}_\pi, \\ \Delta_0^- &= \mathcal{U}_\pi, & \Delta_n^- &= T^{-1}\Delta_{n-1}^- \cap \mathcal{U}_\pi,\end{aligned}$$

is such that $\lim_{n \rightarrow \infty} \nu(\Delta_n^\pm) = 0$.

Comment. In the case of even periodic potential $V(x)$ the relation (12) implies that $\nu(\Delta_n^+) = \nu(\Delta_n^-)$ for any n . Therefore in order to verify Hypothesis 3 in this case it is enough to check the condition $\lim_{n \rightarrow \infty} \nu(\Delta_n^+) = 0$ only.

It follows from Theorem 4 that if Hypotheses 1–3 hold then there exists one-to-one correspondence between all bounded in \mathbb{R} solutions of Eq. (9) and the sequences from Ω^N which can be regarded as *codes* for these solutions. The “coding” sequence from Ω^N consists of numbers i of D_i in the order the orbit “visit” them. In the next section we describe the results of numerical study of Eq. (9) with cosine potential (8) i.e. for the equation

$$u_{xx} + (\mu - A \cos 2x)u - u^3 = 0. \quad (13)$$

We present numerical arguments that Hypotheses 1–3 hold for vast areas in the plane of parameters (μ, A) .

4 Steady States with Cosine Potential

First, let us remind some facts from the theory of linearized equation

$$u_{xx} + (\mu - A \cos 2x)u = 0 \quad (14)$$

which is the Mathieu equation [17]. In the plane of parameters (μ, A) there exist zones where all the solutions of Eq. (14) are bounded (*bands*) and where all of them are unbounded (*gaps*). Figure 2 reproduces classical picture of gap/band structure for Eq. (14) in the plane (μ, A) . It is known that this structure also play an important role in the theory of nonlinear equation (13) (see e.g. [1]). In terms of Poincaré map T associated with Eq. (13), if the point (μ, A) is situated in a band then the origin $O(0, 0)$ is an elliptic fixed point for T and if (μ, A) lies in a gap then $O(0, 0)$ is a hyperbolic fixed point for T .

The numerical study of Eq. (13) was fulfilled using interactive software elaborated specifically for this equation. It allows to visualize orbits of map T , to seek for fixed points of T^n , $n = 1, 2, \dots$, to scan the plane of initial data (u, u') in order to construct the sets \mathcal{U}_L^\pm and \mathcal{U}_L , to measure the areas of these sets and possesses some other useful features.

Let us now summarize the results of the numerical study.

Orbits for T . Figure 3 represents successive iterations of the map T for various initial points. Vast empty areas outskirts of the central region in panels a-d correspond to collapsing solutions Eq. (13). For these points the map T is not defined.

The sets \mathcal{U}_π^\pm and \mathcal{U}_π . In order to visualize the sets \mathcal{U}_L^\pm numerical scanning of the initial data plane (u, u') was fulfilled. Numerical study shows that for any

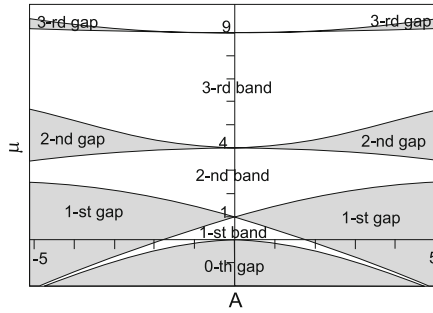


Fig. 2 Band/gap structure for the Mathieu equation

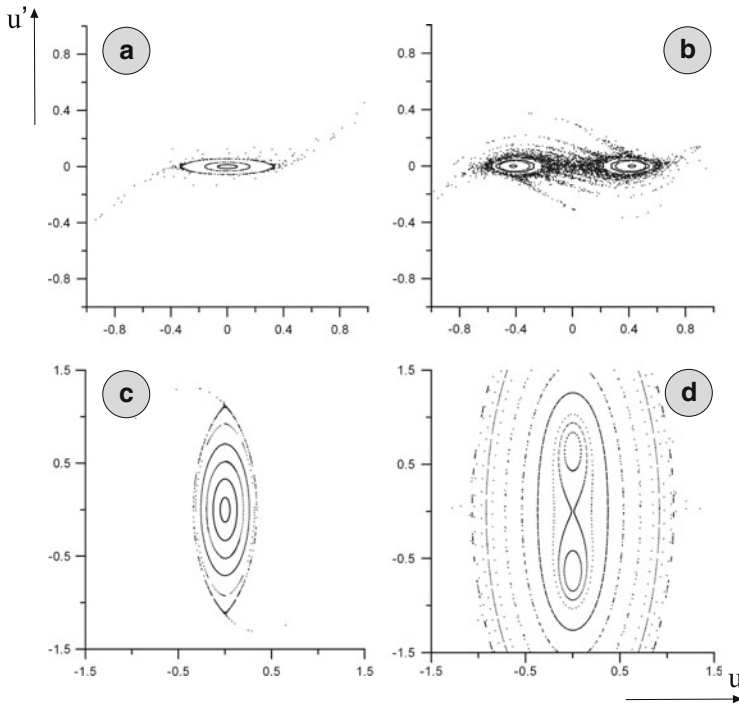


Fig. 3 Orbits for various initial points in the plane of initial data (iterated Poincaré maps), $A = -1$. (a) $\mu = 0$, 1st band; (b) $\mu = 0.6$, 1st gap; (c) $\mu = 2$, 2nd band; (d) $\mu = 4.05$, 2nd gap. Vast empty areas outskirts the central region in panels a–d correspond to collapsing solutions of Eq. (13). For these data the map T is not defined

values of parameters μ and A the sets \mathcal{U}_π^\pm are *infinite curvilinear strips*. The typical shapes of the sets \mathcal{U}_π^\pm for Eq. (13) are shown in Fig. 4. The boundary of \mathcal{U}_π^+ is represented by two continuous curves α^\pm . The curve α^+ consists of the such points (u_0, u'_0) that the solution $u(x)$ of the Cauchy problem for Eq. (13) with

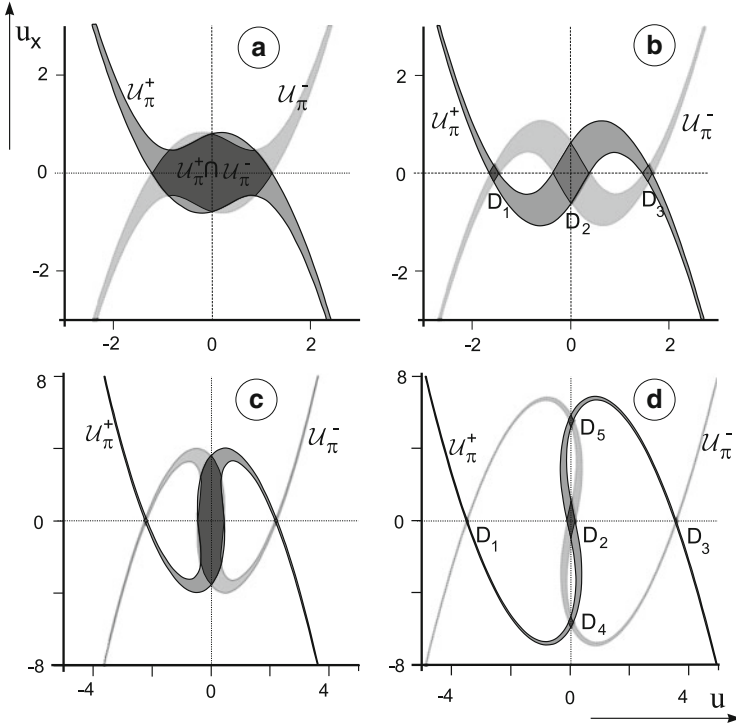


Fig. 4 The sets \mathcal{U}_π^+ and \mathcal{U}_π^- for the parameters μ and A lying in the first (panels **a** and **b**) and the second (panels **c** and **d**) gaps. The parameters are: (a) $\mu = 1$, $A = -1$; (b) $\mu = 1$, $A = -3$; (c) $\mu = 4$, $A = -4$; (d) $\mu = 4$, $A = -10$. The sets were obtained numerically by scanning of initial data plane for Eq. (13). In dark the areas $\mathcal{U}_\pi = \mathcal{U}_\pi^+ \cap \mathcal{U}_\pi^-$ are shown

initial data $u(0) = u_0$, $u'(0) = u'_0$ collapses at $x = \pi$ and $\lim_{x \rightarrow \pi} u(x) = +\infty$. At the curve α^- the solution $u(x)$ of the corresponding Cauchy problem obeys the condition $\lim_{x \rightarrow \pi} u(x) = -\infty$. Similarly, the boundary of \mathcal{U}_π^- is represented by two continuous curves β^\pm . The curves β^\pm consists of the points (u_0, u'_0) such that the solution $u(x)$ of the Cauchy problem for Eq. (13) with initial data $u(0) = u_0$, $u'(0) = u'_0$ collapses at $x = -\pi$ and $\lim_{x \rightarrow -\pi} u(x) = \pm\infty$. It is important that the set $\mathcal{U}_\pi = \mathcal{U}_\pi^+ \cap \mathcal{U}_\pi^-$ may consist of *several disjoint components*, as it is in panel b and d of Fig. 4.

The sets $\mathcal{U}_{n\pi}^\pm$. Figure 5 exhibits the sets $\mathcal{U}_{6\pi}^+$ for $\mu = 1$ and various values of A . The sets $\mathcal{U}_{6\pi}^-$ are the reflection of the sets $\mathcal{U}_{6\pi}^+$ with respect to u axes. In Fig. 5 the sets $\mathcal{U}_{6\pi}^\pm$ have quite a complex layered structure. The structure of $\mathcal{U}_{n\pi}^\pm$ becomes more sophisticated as n grows resembling *fractals*. The situation is similar to one described in [18] for Eq. (9) in the case of delta-comb potential (see Fig. 7 in Ref. [18]).

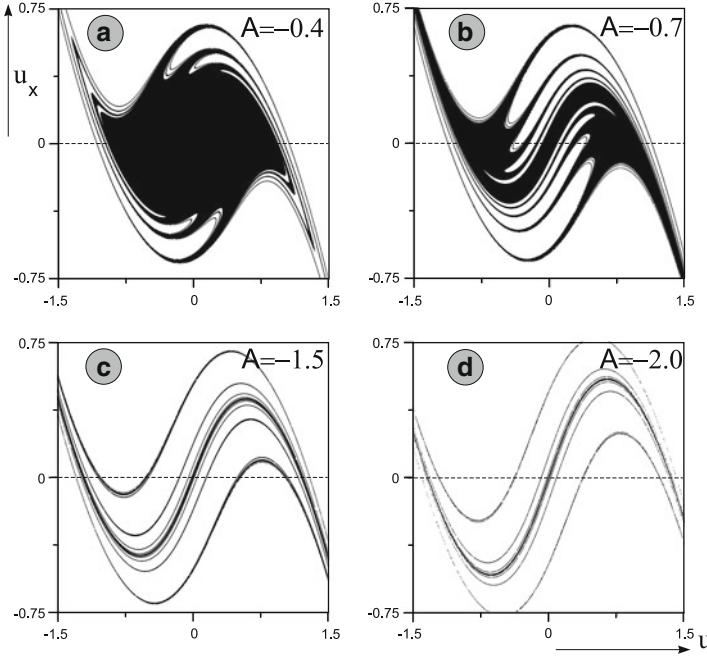


Fig. 5 The sets $\mathcal{U}_{6\pi}^+$ and $\mathcal{U}_{6\pi}^-$. In all the cases $\mu = 1$ and (a) $A = -0.4$; (b) $A = -0.7$; (c) $A = -1.5$; (d) $A = -2.0$. The steps of scanning with respect to u and u' are 0.0005 and 0.0002 correspondingly

4.1 Hypothesis 1

In all the cases the sets \mathcal{U}_{π}^+ and \mathcal{U}_{π}^- shown in Fig. 4 are *curvilinear strips*. We found that this is a *general feature* of Eq. (13) for all parameters μ and A which we considered. The shapes of the strips \mathcal{U}_{π}^{\pm} may be quite complex and their intersection \mathcal{U}_{π} may consist of different number of disjoint sets. Since the strips \mathcal{U}_{π}^+ and \mathcal{U}_{π}^- are related to each other by symmetry with respect to u axis, the typical situation is that \mathcal{U}_{π} consists of *some number of curvilinear deltoids* (see Fig. 4, panels b and d) which are symmetrical with respect to u or u' axes.

Figure 6 shows the regions in the parameter plane (μ, A) where such decomposition of \mathcal{U}_{π} takes place (the half-plane $A < 0$ is depicted). In the area above the curve $N = 3$ and below the curve $N = 5$ the set \mathcal{U}_{π} consists of three connected components, in the area above the curve $N = 5$ it consists of five connected components etc. It is important that *these components are islands* (in the sense of Sect. 3.2) in the areas between the marked curves and upper boundaries of the gaps, shown in Fig. 6 in dark.

The possible numbers of islands are related (indirectly) to numbers of fixed points of the Poincaré map T . In its turn the number of fixed points of T is

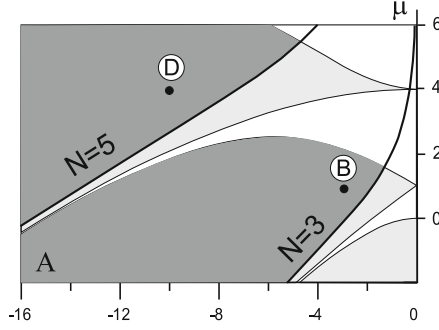


Fig. 6 The plane of parameters (μ, A) with band and gap zones. The boundaries of the regions where \mathcal{U}_π is disjoined in three (the curve $N = 3$) or five (the curve $N = 5$) connected components are shown. These components are islands (in the sense of Sect. 3.2) in dark areas between the marked curves and upper boundaries of the corresponding gaps. The points corresponding to panels b and d of Fig. 4 are marked

determined by the number of band or gap where the point (μ, A) is situated in the plane of parameters. More detailed analysis of these relations is an interesting issue for a further study.

4.2 Hypothesis 2

Let DT_p be the operator of linearization of T at point p . Let

$$\mathbf{e}_1 = \begin{pmatrix} 1 \\ 0 \end{pmatrix}; \quad \mathbf{e}_2 = \begin{pmatrix} 0 \\ 1 \end{pmatrix}. \quad (15)$$

Define the functions

$$\begin{aligned} g_1(p) &= (DT_p \mathbf{e}_1, \mathbf{e}_1) \cdot (DT_p \mathbf{e}_2, \mathbf{e}_1), \\ g_2(p) &= (DT_p \mathbf{e}_1, \mathbf{e}_2) \cdot (DT_p \mathbf{e}_2, \mathbf{e}_2). \end{aligned}$$

The way to verify the conditions of Hypothesis 2 is based on the following statement:

Theorem 5. Assume that the potential $V(x)$ is even and the following conditions hold:

- \mathcal{U}_π^+ is an infinite curvilinear strips;
- $\mathcal{U}_\pi^+ \cap \mathcal{U}_\pi^- = \mathcal{U}_\pi = \bigcup_{i=1}^N D_i$ where D_i are nonintersecting islands;
- For each pair (i, j) , if

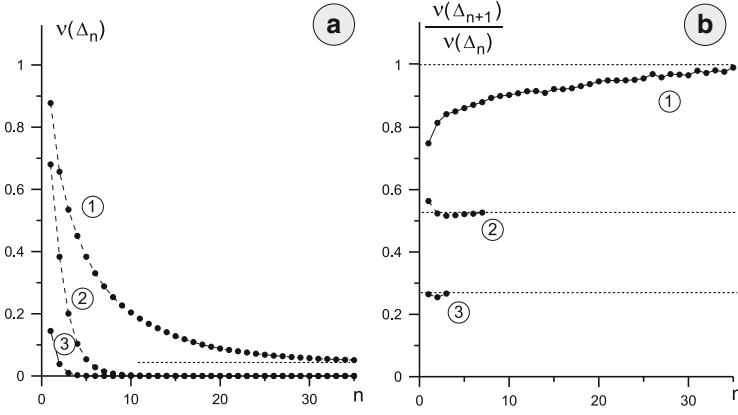


Fig. 7 Panel **a**: The area of the set Δ_n^+ versus n for $\mu = 1$ and (1) $A = -0.7$, (2) $A = -1.2$ and (3) $A = -2$. Panel **b**: The ratio $R_n = v(\Delta_{n+1}^+)/v(\Delta_n^+)$ for the same values of μ and A . Only few points are shown in panel **b** for the cases (2) and (3) since accuracy of calculations drastically falls due to division to small denominator

- β_i^\pm are graphs of monotone increasing functions then for any $p \in T^{-1}D_j \cap D_i$ the relations $g_1(p) > 0$, $g_2(p) > 0$ hold;
- β_i^\pm are graphs of monotone decreasing functions then for any $p \in T^{-1}D_j \cap D_i$ the relations $g_1(p) < 0$, $g_2(p) < 0$ hold.

Then the conditions of Hypothesis 2 take place.

The proof of Theorem 5 is presented in [14]. It is convenient to incorporate the calculation of the values $g_1(p)$ and $g_2(p)$ in general cycle of numerical scanning in the plane (u, u') . Our numerical study indicates that *Hypotheses 2 holds for the parameters μ and A lying in the dark areas in Fig. 6.*

4.3 Hypothesis 3

The computation of $v(\Delta_n^+)$ was incorporated in the general cycle of numerical scanning of the plane (u, u') . The numerical results for some μ and A are depicted in Fig. 7. It follows from Fig. 7 that Hypothesis 3 is valid not in all considered cases.

A natural obstruction for the conditions of Hypothesis 3 to hold is presence of elliptic fixed points of T or elliptic periodic orbits (cycles) of T . Due to KAM theory in vicinity of an elliptic fixed point (or cycle) generically there exists a set of positive measure that consists of points which do not leave this vicinity after any number of iterations of T . This means that Hypothesis 3 is not valid when the parameters μ and A are in band zones, because of presence of elliptic fixed point $O(0, 0)$ of T . This situation takes place in the case (1) in Fig. 7.

When the point (μ, A) is situated in a gap, the point $O(0, 0)$ becomes a hyperbolic fixed point of T . However there exists some region in the gap adjacent to its lower boundary where elliptic periodic orbits of T persist. They are related to the fixed point $O(0, 0)$ by means of a sequence of period doubling bifurcations. The cascade of bifurcations is similar to the period doubling cascade described in [18] for Eq. (9) with delta-comb potential. At the same time if μ and A are situated in dark zones in Fig. 6 the computations give a numerical evidence that Hypothesis 3 holds. Moreover, our results allow to assume exponential convergence of $v(\Delta_n^+)$ to zero. This takes place for the cases (2) and (3), see panel b of Fig. 7.

4.4 Examples

Let us give some examples how the coding technique can be applied.

Example 1. Let the parameters (μ, A) belong to dark zone in the first gap, see Fig. 6. Then all the bounded in \mathbb{R} solutions of Eq. (13) can be coded by bi-infinite sequences of three symbols. These symbols mark entering of orbit into D_1 , D_2 and D_3 correspondingly. They may be chosen as “+”, “0” and “−”. Then

- There exists well-known solution $u(x)$ in the form of bright gap soliton, localized in one well of the potential. This solution corresponds to the code $(\dots 00 + 00 \dots)$. Also there exist the gap soliton solution $-u(x)$ with the code $(\dots 00 - 00 \dots)$;
- There exists two π -periodic solutions of Eq. (13) with codes $(\dots + + + \dots)$ and $(\dots - - - \dots)$;
- There exists infinitely many dark soliton type solution corresponding to the codes $(\dots - - - + + + \dots)$, $(\dots - - - 0 + + + \dots)$, etc;
- There exists “domain wall”-type solutions corresponding to the codes $(\dots 000 + + + \dots)$, $(\dots - - - 000 \dots)$. These objects were found to exist in the case of GPE with attractive nonlinearity [12]. So, they exist in the case of repulsive nonlinearity also.

Example 2. Assume again that the parameters (μ, A) belong to dark zone in the first gap. Consider boundary value problem for Eq. (13) on the interval $[-4\pi, 0]$ with Neumann boundary conditions at $x = -4\pi$ and $x = 0$. These solutions can be regarded as reductions to the interval of length 4π of periodic solutions with period 8π which satisfy additional symmetry conditions

$$u(x) = u(-x); \quad u(-4\pi + x) = u(-4\pi - x).$$

The codes for these solutions are of the form

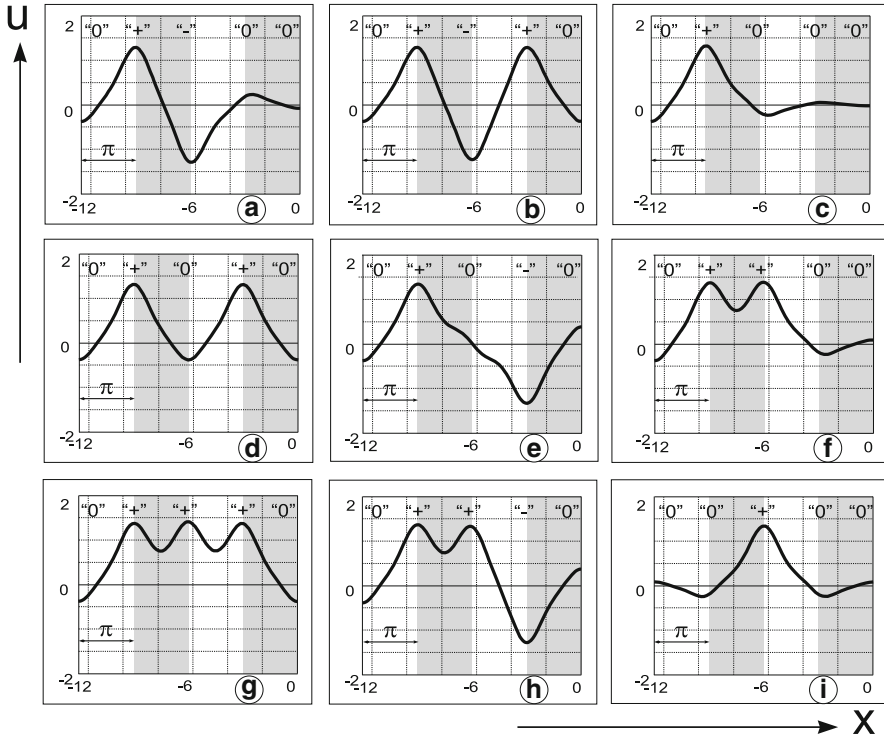


Fig. 8 The solutions of Eq. (13) ($A = -2$, $\mu = 1$) on the interval $[-4\pi, 0]$ with Neumann boundary conditions at $x = -4\pi$ and $x = 0$. The codes (the blocks $(\theta_1\theta_2\theta_3\theta_4\theta_5)$) are: **a**: (0 + -00); **b**: (0 + - +0); **c**: (0 + 000); **d**: (0 + 0 + 0); **e**: (0 + 0 - 0); **f**: (0 + +00); **g**: (0 + + + 0); **h**: (0 + + - 0); **i**: (00 + 00)

$$(\dots \theta_5 \theta_4 \theta_3 \theta_2 \underbrace{\theta_1 \theta_2 \theta_3 \theta_4 \theta_5 \theta_4 \theta_3 \theta_2}_{\text{the period}} \theta_1 \theta_2 \theta_3 \theta_4 \theta_5 \dots),$$

where θ_i , $i = 1 \div 5$, is one of the symbols “+”, “0” or “-”. Therefore there are $3^5 = 243$ solutions of this type. In Fig. 8 nine of these solutions are depicted for $A = -2$, $\mu = 1$. All the solutions shown in Fig. 8 have the codes with “0” as the first and last symbols on the semi-period. Therefore they can be regarded as approximations for localized modes which have the domain of localization of length 4π . These localized modes correspond to the codes

$$(\dots 00 \theta_2 \theta_3 \theta_4 00 \dots).$$

There are 27 sequences of this type but only 10 of them are different in the sense that they are not related to each other by symmetry reductions. All of them, except zero solution with the code $(\dots 00000 \dots)$ are presented in Fig. 8.

5 Conclusion

In this contribution we describe an approach for classification of nonlinear modes covered by Eq. (5) with periodic potential $V(x)$ and repulsive nonlinearity $g = 1$. The approach is based on the fact that “great part” of the solutions for Eq. (5) are collapsing i.e. they tend to infinity at some point of x axis. We analyze the location of initial data for solutions which does not exhibit collapsing behavior within the period of potential (the sets \mathcal{U}_π^\pm). Then we applied methods of symbolic dynamics to study transformations of these sets under the action of Poincaré map T . As a result, we formulate three hypotheses which guarantee one-to-one correspondence between all bounded in \mathbb{R} solutions of Eq. (5) and the set of bi-infinite words of N -symbol alphabet. The number N is determined by the parameters of Eq. (5). These sequences can be regarded as codes for the solutions of Eq. (5). For a given $V(x)$ the hypotheses should be verified numerically. We report on numerical verification of hypotheses for the case of cosine potential, i.e., for Eq. (13), and indicate regions in the plane of parameters (μ, A) where this coding is possible.

The approach may be applied to various versions of Eq. (1) and it may be extended in many directions. In particular, preliminary studies show that it can be applied with minor modifications to the case of Eq. (7) with $g_2 < 0$ and cosine potential. The shapes of the sets \mathcal{U}_π^\pm in this case are similar to ones described above for Eq. (5). Other interesting issues for further studies, in our opinion, are as follows:

- Is it possible to modify the method described above to study the dynamics in the case of partially overlapping islands?
- What peculiarities can appear in the situation when the potential $V(x)$ has several wells of different depth on each period?
- What type of coding can be used to describe the nonlinear modes for Eq. (6)?

Acknowledgements The work of authors was supported by Russian federal program “Scientific and educational personnel of the innovative Russia”, grant 14.B37.21.1273.

References

1. V.A. Brazhnyi, V.V. Konotop, Mod. Phys. Lett. B, **18**, 627 (2004)
2. L.P. Pitaevskii, Phys. Usp. **49**, 333 (2006)
3. O. Morsch, M. Oberthaler, Rev. Mod. Phys. **78**, 179 (2006)
4. L. Pitaevskii, S. Stringari, *Bose-Einstein condensation* (Clarendon Press, Oxford, 2003)
5. G.L. Alfimov, V.V. Konotop, M. Salerno, Europhys. Lett. **58**, 7 (2002)
6. F.K. Abdullaev, M. Salerno, Phys. Rev. A **72**, 033617 (2005)
7. G.L. Alfimov, V.V. Konotop, P. Pacciani, Phys. Rev. A **75**, 023624 (2007)
8. P.J.Y. Louis, E.A. Ostrovskaya, C.M. Savage, Yu.S. Kivshar, Phys. Rev. A **67**, 013602 (2003)
9. V.V. Konotop, M. Salerno, Phys. Rev. A **65**, 021602 (2002)
10. D.E. Pelinovsky, A.A. Sukhorukov, Yu.S. Kivshar, Phys. Rev. E **70**, 036618 (2004)
11. B. Wu, Q. Niu, Phys. Rev. A **64**, 061603(R) (2001)

12. P.G. Kevrekidis, B.A. Malomed, D.J. Frantzeskakis, A.R. Bishop, H. Nistazakis, R. Carretero-González, *Math. Comput. Simul.* **69**, 334 (2005)
13. T.J. Alexander, E.A. Ostrovskaya, Yu.S. Kivshar, *Phys. Rev. Lett.* **96**, 040401 (2006)
14. G.L. Alfimov, A.I. Avramenko, *Physica D* **254**, 29 (2013)
15. P.J. Torres, *Nonlinear Anal.* **65**, 841 (2006)
16. S. Wiggins, *Introduction to applied dynamical systems and chaos* (Springer, New York, 1990)
17. M. Abramowitz, I. Stegun (eds.), *Handbook of mathematical functions* (Dover, New York, 1970)
18. D. Witthaut, K. Rapedius, H.J. Korsch, *J. Nonlinear Math. Phys.* **16**, 207 (2009)

Localized Excitations in Nonlinear Complex Systems

Current State of the Art and Future Perspectives

Carretero-González, R.; Cuevas-Maraver, J.;

Frantzeskakis, D.; Karachalios, N.; Kevrekidis, P.;

Palmero-Acebedo, F. (Eds.)

2014, XX, 432 p. 175 illus., 117 illus. in color.,

Hardcover

ISBN: 978-3-319-02056-3